JACS
JOURNAL OF THE AMERICAN CHEMICAL SOCIETY

ARTICLE

pubs.acs.org/JACS

Hydrogen Spillover in Pt-Single-Walled Carbon Nanotube Composites: Formation of Stable C−H Bonds

Ranadeep Bhowmick,[†] Srivats Rajasekaran,[§] Daniel Friebel,[§] Cara Beasley,[†] Liying Jiao,[‡] Hirohito Ogasawara,[§] Hongjie Dai,[‡] Bruce Clemens,[†] and Anders Nilsson*[,§]

[†]Department of Material Science and Engineering and [‡]Department of Chemistry, Stanford University, Stanford, California 94305, United States

[§]Stanford Synchrotron Radiation Lightsource, SLAC National Accelerator Laboratory, 2575 Sand Hill Road, Menlo Park, California 94025, United States

Supporting Information

ABSTRACT: Using in situ electrical conductivity and ex situ X-ray photoelectron spectroscopy (XPS) measurements, we have examined how the hydrogen uptake of single-walled carbon nanotubes (SWNTs) is influenced by the addition of Pt nanoparticles. The conductivity of platinum-sputtered single-walled carbon nanotubes (Pt-SWNTs) during molecular hydrogen exposure decreased more rapidly than that of the corresponding pure SWNTs, which supports a hydrogenation mechanism facilitated by "spillover" of dissociated hydrogen from the Pt nanoparticles. C 1s XPS spectra indicate that the Pt-SWNTs store hydrogen by means of chemisorption, that is, covalent C−H bond formation: molecular hydrogen charging at elevated pressure (8.27 bar) and room temperature yielded Pt-SWNTs with up to 16 ± 1.5 at. % sp^3-hybridized carbon atoms, which corresponds to a hydrogen-storage capacity of 1.2 wt % (excluding the weight of Pt nanoparticles). Pt-SWNTs prepared by the Langmuir−Blodgett (LB) technique exhibited the highest Pt/SWNT ratio and also the best hydrogen uptake.

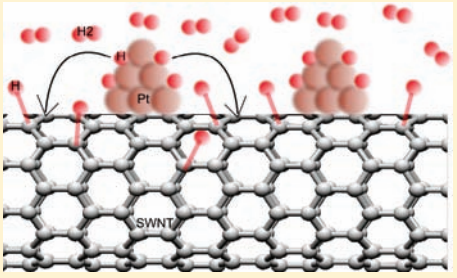

1. INTRODUCTION

The proposal of Dillon et al.[1] that carbon nanotubes (CNTs) could store large quantities of hydrogen by physisorption has led many groups to investigate the possibility of CNT-based hydrogen-storage materials. While it remains to be shown that significant amounts of hydrogen can be stored in CNTs using physisorption, theoretical predictions suggest that it is possible to achieve 100% hydrogenation of SWNTs (i.e., one H atom per one C atom) through a chemisorption mechanism in which stable C−H bonds are formed.[2] Such a mechanism would involve the breaking of the C−C π-bonds and the conversion of C atoms from sp^2 to sp^3 hybridization upon coordination with hydrogen. It has also been shown that the C−H bonds thus formed would be stable if the CNTs were of optimum curvature.[2] One could therefore systematically tune the chemical reactivity of CNTs toward hydrogen by changing their diameter.[3]

SWNTs treated with hydrogen plasma were found to exhibit increased resistance arising from a widened band gap;[4] this is consistent with the formation of C−H chemical bonds. Previous works have shown that hydrogen plasma can induce C−H bonds in SWNTs, which were detected using valence band photoemission[5] and infrared spectroscopies.[6] Moreover, X-ray absorption (XAS) and X-ray photoelectron (XPS) spectroscopies have recently shown that atomic hydrogen interacts reversibly with carbon atoms in CNTs, yielding stable C−H bonds that can be removed by heating to 200−300 °C.[7−9] By providing information about the presence of C−H bonds (through the C 1s shift) and allowing for the quantification of the number of such bonds per carbon atom,[7−10] XPS studies have demonstrated that for specific SWNTs an atomic hydrogen source can hydrogenate almost 100% of the nanotubes.[9] These results suggest that by chemisorbing hydrogen on SWNTs, it may be possible to approach hydrogen storage capacities of 7.7 wt % (corresponding to 100% hydrogenation), which would render such materials technologically viable for hydrogen-storage devices.

While previous studies have generated large concentrations of C−H bonds using an atomic hydrogen source[7−9] and hydrogen plasma source,[5] the practical implementation of hydrogen storage in CNTs requires the development of low-barrier pathways for hydrogen dissociation. One potential pathway could be to take advantage of the "spillover" mechanism, in which molecular hydrogen spontaneously dissociates on a metal catalyst (usually platinum, palladium, ruthenium, or nickel[11]) in intimate contact with the carbon support, producing mobile H atoms that spill over onto the CNTs. However, despite efforts by several groups to address the role of spillover in the hydrogen uptake of carbon nanofibers, activated carbon, and other carbon-based materials,[12−16] both the validity of the spillover mechanism and the possibility of significant hydrogen storage in CNTs remain

Received: January 14, 2011
Published: March 23, 2011

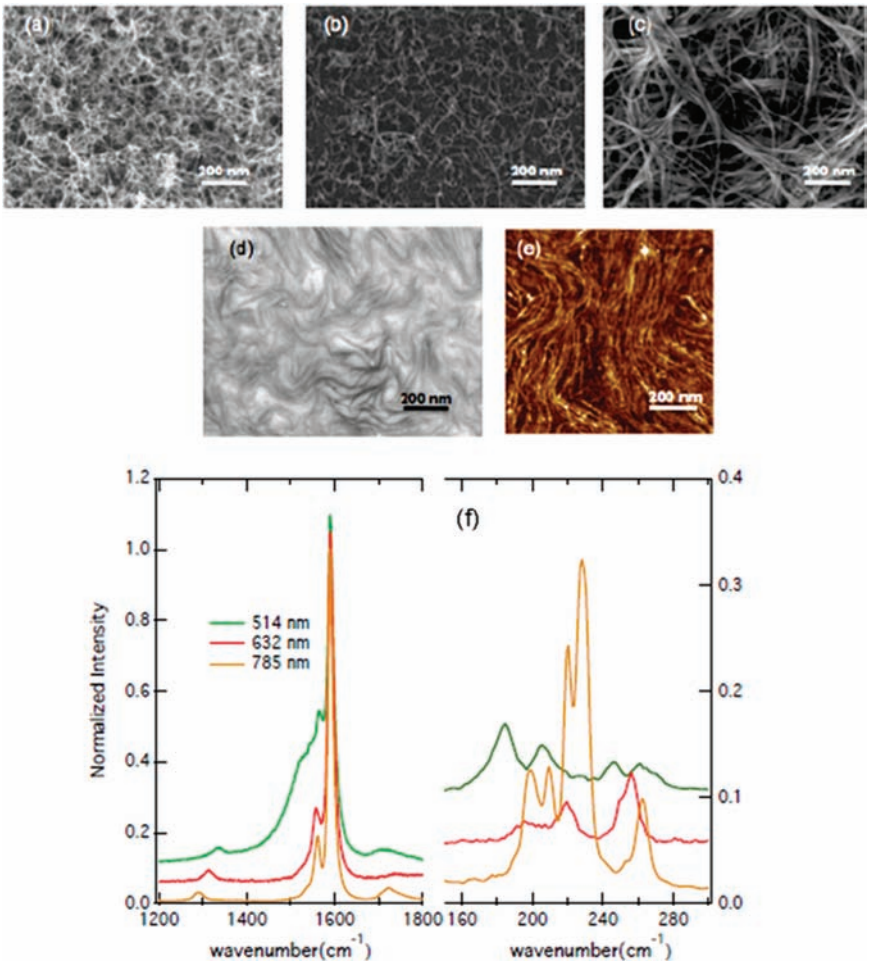

Figure 1. SEM images of (a) dense and (b) sparse distributions of CVD-grown SWNTs, (c) spincast HiPCO SWNTs, and (d) an LB film. (e) AFM image of an LB film. (f) Representative Raman spectrum of HiPCO SWNTs.

controversial because very few studies have specifically examined whether C−H chemical bonds could form through a spillover mechanism: to the best of our knowledge, the only such experiments are inelastic neutron-scattering (INS) performed on metal−carbon fuel cell catalysts dosed with hydrogen, which probed dissociated hydrogen species adsorbed onto the to the carbon support.[17] Similar INS experiments performed on carbon fibers sputtered with palladium provide evidence of the spillover mechanism.[18] Other experiments validating the spillover mechanism are the study of electrical conductivity and infrared absorption (IR) studies[19] and isotope exchange TPD experiments[20] for hydrogen uptake in metal/carbon composites. To further the potential of nanotubes as hydrogen-storage materials using molecular hydrogen as the precursor source for hydrogen loading at nearly ambient conditions, it is therefore important to establish clear evidence of a spillover mechanism with a metal catalyst.

In the present Article, we report that on the basis of in situ electrical conductivity and ex situ XPS measurements, a hydrogen spillover indeed takes place in Pt-SWNT composites. Conductivity measurements clearly show a steady increase in the resistance of the Pt-SWNTs during exposure to molecular hydrogen gas, which is consistent with a transition of the carbon atoms in the SWNTs from sp^2 to sp^3 hybridization. Moreover, XPS measurements confirm that up to 16 ± 1.5 at. % of the carbon atoms in the composites rehybridize from sp^2 to sp^3; these effects are most enhanced for SWNTs that are dispersed into small bundles using the Langmuir−Blodgett method,[21] which yields the highest Pt coverage on the SWNT surface.

2. EXPERIMENTAL DETAILS

2.1. Sample Preparation. The SWNTs employed in the present study were from two different sources: (i) CVD-grown SWNTs, and (ii) commercially procured HiPCO SWNTs. The CVD-grown samples were grown in an atmospheric chemical-vapor deposition (CVD) system utilizing isopropanol as the carbon source. The growth temperature was varied from 700 to 800 °C to change the density of SWNTs in the film and the overall film thickness. Different gas flow rates were also used to influence the density and thickness of the films produced. To generate samples that could be used directly in subsequent conductivity and XPS measurements, the SWNTs were grown on a 2 Å thick film of cobalt metal deposited on silicon oxide wafers with 50 nm of oxide; see Figure 1a and b. The advantage of this preparation method is that it was not necessary to use any further treatment procedure; that is, we did not need to mix the SWNTs with any alcohol or surfactant to obtain a well-dispersed film.

The HiPCO SWNTs were used to prepare samples by two different methods. For the thicker samples, the SWNTs were dispersed in isopropanol (1 mg/10 mL), sonicated for 15 min, and then spin-cast

dx.doi.org/10.1021/ja200403m |J. Am. Chem. Soc. 2011, 133, 5580–5586

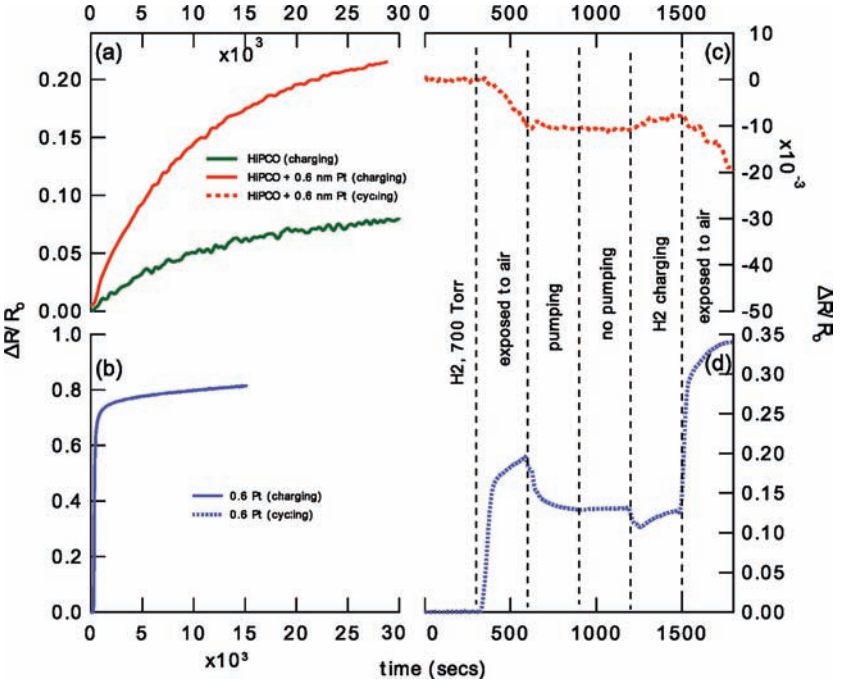

Figure 2. (a) Change in resistance of Pt-HiPCO CNT composites upon molecular hydrogen exposure with and without Pt nanoparticles, (b) change in resistance of a polycrystalline Pt film upon exposure to hydrogen, (c) resistance changes in the Pt-CNTs composites under cycling the hydrogen exposure pressure, and (d) cycling for polycrystalline Pt film.

on a quartz slide (Figure 1c). Before Pt deposition, the samples were annealed in an evacuated chamber at 250 °C for 1 h to evaporate residual alcohol. To maintain uniformity of the samples, the same deposition steps were rigorously followed each time. While the preparatory ease of this method is a major advantage, it yielded thick films composed of bundled SWNTs, which consequently had the lowest Pt/SWNT ratio of all the films we prepared.

The optimal SWNT film for hydrogen storage would be a uniform monolayer of unbundled SWNTs; such a film is expected to allow for the highest loading with Pt and therefore the highest hydrogen-storage capacity on a weight-percent basis. To unbundle the tubes, we performed a density-gradient-centrifugation (DGC) rate (zonal) separation for sodium-cholate suspended SWNTs through an iodixanol step-gradient at 300 000*g*. This method separates nanotubes by mass, with fractions rich in single tubes floating on top of the column and bundles settling at the lower parts of the centrifuge column; long, individual SWNTs can be obtained from the top fractions and characterized by spectroscopic methods. Xiaolin et al.[21] used individual tubes extracted in this manner to prepare monolayer assemblies of SWNT films by the Langmuir−Blodgett (LB) method, in which SWNTs functionalized by PmPV were dispersed in 1,2-dichloroethane. These authors additionally observed that pressure cycling during LB-film compression facilitates high-degree alignment and packing of SWNTs. Figure 1d and e shows SEM and AFM images of SWNT films prepared on silicon with a thin layer of native oxide using the LB technique. Once the LB films formed, they were calcinated to remove organic solvents, surfactants, and any other remaining contaminants. One disadvantage of this technique is that the SWNTs undergo a number of processing steps that could give rise to organic contaminants that persist even after calcination; spectroscopic data from LB films must therefore be interpreted with some caution.

By comparison of the Raman spectra of HiPCO SWNTs obtained using three different excitation lasers (Figure 1e) with the Kataura plot,[22] we estimate a diameter range for these samples of 0.8−1.6 nm; the estimated diameter range of the CVD-grown SWNTs is similar.

For deposition of Pt nanoparticles onto the nanotube samples, the SWNT is first annealed at 250 °C in a vacuum. Sputter deposition of Pt was performed in a load-locked chamber at Ar pressures of $1.5-5 \times 10^{-3}$ Torr with a target bias in the several hundred volts range. The deposition rate was monitored with a quartz crystal microbalance, which was calibrated using the actual film thickness measured by X-ray reflectivity. The reported Pt thicknesses were the nominal values assuming the Pt had deposited as a uniform thickness film. A pure, polycrystalline Pt film was also prepared by sputter depositing of a 6 Å thick layer onto an oxidized Si wafer.

2.2. Electrical Conductivity Measurements. To study the change in conductivity of the Pt-sputtered SWNT films during hydrogen charging, in situ four-probe tests on SWNTs deposited onto quartz were performed. A constant current was passed through the outer probes, and the potential difference between the two inner probes was monitored as a function of charging time. By using four probes rather than a conventional two-probe setup, any changes in measured conductivity arising from variations in the contact resistance were eliminated. Platinum metal pads were sputter deposited on the SWNT film, to facilitate good electrical contact with the four probes. (More information about experimental setup for this study can be found in the Supporting Information.)

2.3. XPS Measurements. Ex situ XPS measurements of the C 1s and Pt 4f core-levels were performed on Pt-SWNT composites before and after hydrogen charging to establish the presence of C−H bonds.[7,8] LB films and CVD-grown SWNT films were chosen for the XPS studies, because they showed the largest hydrogen uptake based on our conductivity studies.

The samples were annealed overnight in an evacuated chamber at 250 °C, and reference C 1s and Pt 4f XPS spectra of these clean samples were recorded. The clean Pt-SWNTs were subsequently exposed to molecular hydrogen at a pressure of 8.27 bar for 6 h. After the hydrogen treatment, the samples were placed inside a glovebag containing forming gas (5% H_2/95% N_2) to minimize exposure to air while transferring the samples to the XPS chamber for analysis. The XPS measurements were

dx.doi.org/10.1021/ja200403m |*J. Am. Chem. Soc.* 2011, 133, 5580–5586

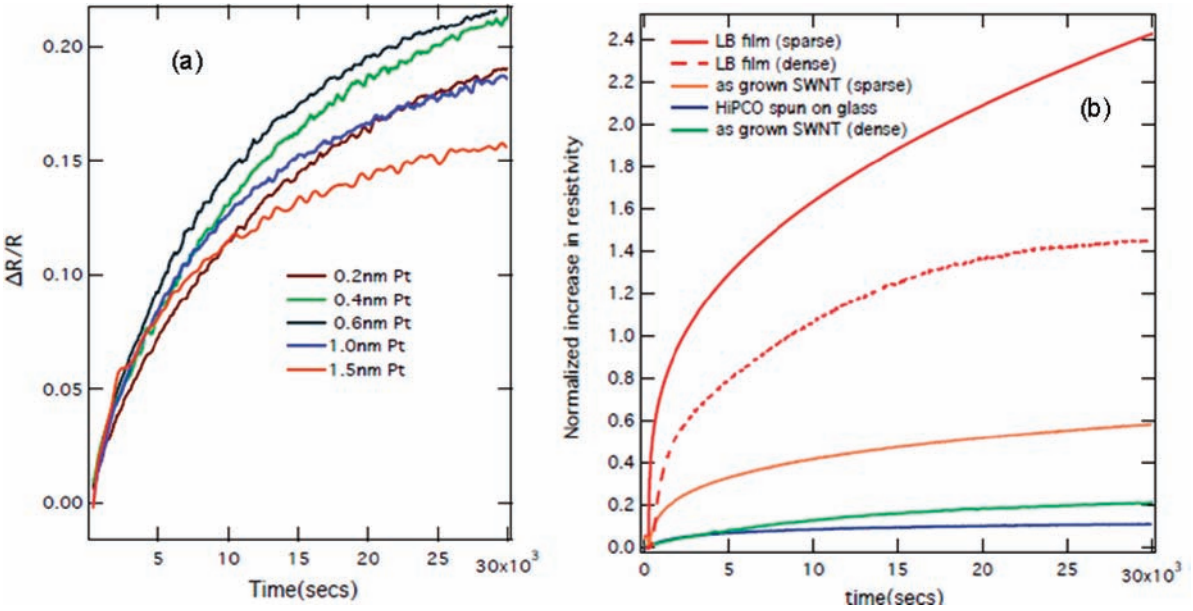

Figure 3. (a) Change in resistance of Pt-SWNTs with different nominal thicknesses of Pt. (b) Change in resistance of different SWNT films with the same nominal thickness of Pt (6 Å).

conducted at the elliptical-undulator beamline 13-2 of the Stanford Synchrotron Radiation Lightsource in a UHV chamber equipped with an electron-energy analyzer (Scienta R3000). All XPS spectra (C 1s and Pt 4f) were recorded with a total resolution of 250 meV and incident photon energy of 400 eV.

3. RESULTS AND DISCUSSION

Figure 2 shows a typical current response for the Pt-HiPCO composite samples under exposure to molecular hydrogen, which were bundled and therefore had the lowest Pt to SWNT ratio. The absolute resistance values of LB films and CVD grown CNT films were 0.9 MΩ and 1.1 KΩ, while those for Pt-LB film composite and Pt-CVD CNT composite were 0.8 MΩ and 1 KΩ. The relative change in resistance ($\Delta R/R_0$) upon hydrogen exposure appears to saturate at a value 4 times greater than that of the corresponding platinum-free HiPCO. Also shown in Figure 2b is the current response of a pure Pt film, which increases rapidly at first before leveling off due to a shift of the Pt Fermi level induced by hydrogen chemisorption. Interestingly, the resistance of the Pt-HiPCO composite continues to increase long after the conductivity of the pure Pt film saturates, which suggests that hydrogen dissociation on the Pt catalyst is not the rate-determining step in the spillover mechanism.

Figure 2c depicts the change in resistance of a Pt-HiPCO composite (with 6 Å Pt) during different cycles of hydrogenation, evacuation, and exposure to air, while Figure 2d shows the results of the same treatment for a pure Pt film. While the resistance of the pure Pt film increases on exposure to air, that of the Pt-HiPCO composite decreases very slightly. The current-response behavior of the pure Pt film may be attributable to the oxidation of chemisorbed hydrogen with oxygen;[23] because this effect could not be seen for Pt-SWNTs, the conductivity change of the Pt-SWNT composites cannot arise from a change in the work function of Pt in a Schottky-type, Pt-SWNT contact diode.

Next, we studied the increase in resistance of the films as a function of the nominal thickness of the sputter deposited Pt. This is shown in Figure 3a. The sputtered Pt film does not wet the SWNT surface, but, as mentioned before, it aggregates into particles. The size and distribution of the particles formed depend on the thickness of the sputtered Pt. This study was done to find the optimal catalyst particle size. With increase in nominal thickness of the catalyst particles, the normalized resistance initially increases to an optimal level, beyond which it decreases. The optimal thickness of the deposited Pt film is 6 Å (corresponding to a particle diameter of 2.05 ± 0.36 nm). This optimal thickness for maximum hydrogen uptake supports the hydrogen uptake measurements with the Sievert's apparatus,[24] where it was observed that the hydrogen uptake by a Pt-SWNT composite film varies linearly with the density of the Pt particles. With an increase in the nominal thickness of the Pt film, the density as well as the size of the catalyst particles increase. Yet, beyond a certain thickness of sputtered film, the Pt particles start agglomerating, thus decreasing the number density of the particles and hence decreasing the extent of H spillover onto the SWNT surface. The particle sizes increase from nominal thickness of 2 Å (corresponding to particle size of 1.14 ± 0.28 nm) to nominal thickness of 6 Å with an increase in number density of Pt nanoparticles on the SWNTs. Around a nominal thickness of 10 Å, reduction in the number density of Pt nanoparticles was observed; see the Supporting Information for TEM morphologies of SWNTS with different amounts of deposited Pt.

For the next experimental set, the nominal thickness of the sputtered Pt was kept constant (6 Å, the optimal nominal thickness determined from the previous set of experiments), but the thickness of the SWNT was varied. For this study, five different SWNT films were used: HiPCO SWNT dispersed in isopropanol and spin-cast on glass, dense and sparse distributions of horizontal SWNT mats grown from Co catalysts on glass, and finally two monolayer thick SWNT films of varying densities assembled by the Langmuir−Blodgett (LB) method. The resistances of the films so prepared are inversely proportional to the thicknesses. It is to be noted that the resistances of the films

dx.doi.org/10.1021/ja200403m |J. Am. Chem. Soc. 2011, 133, 5580–5586

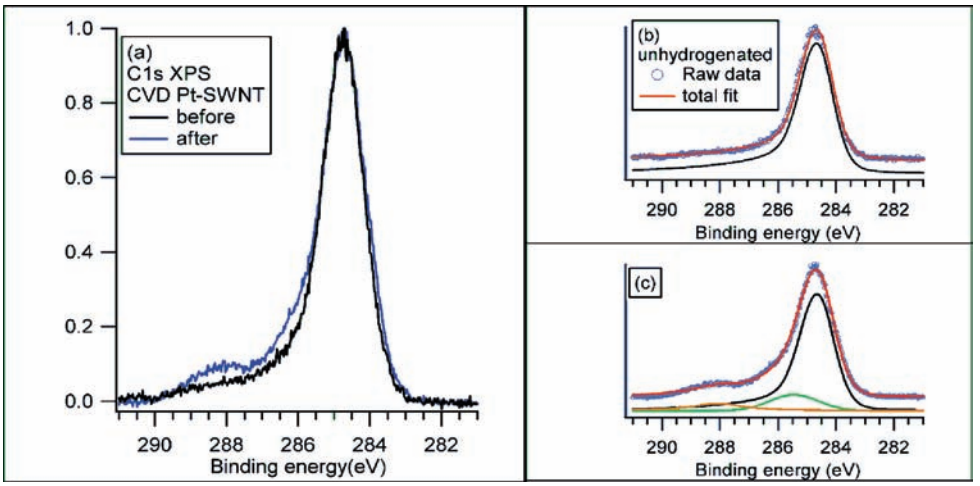

Figure 4. (a) C 1s XPS spectra before (black line) and after (blue line) hydrogen charging for a CVD-grown SWNT film with 6 Å Pt; the peak maxima of both spectra are normalized to enhance differences in the peak shapes. Gaussian−Lorentzian deconvolution (see text for details) of C 1s XPS spectra of the CVD-grown CVD film (b) before and (c) after hydrogen charging: raw data (blue ○); total fit (red line); sp^2-C peak (black line); sp^3-C peak (green line); additional third peak due to hydrogen-induced metal-to-semiconductor transition (orange line). Note that all peaks in (b) and (c) are offset downward from the raw data and the total fit. The incident photon energy is 400 eV.

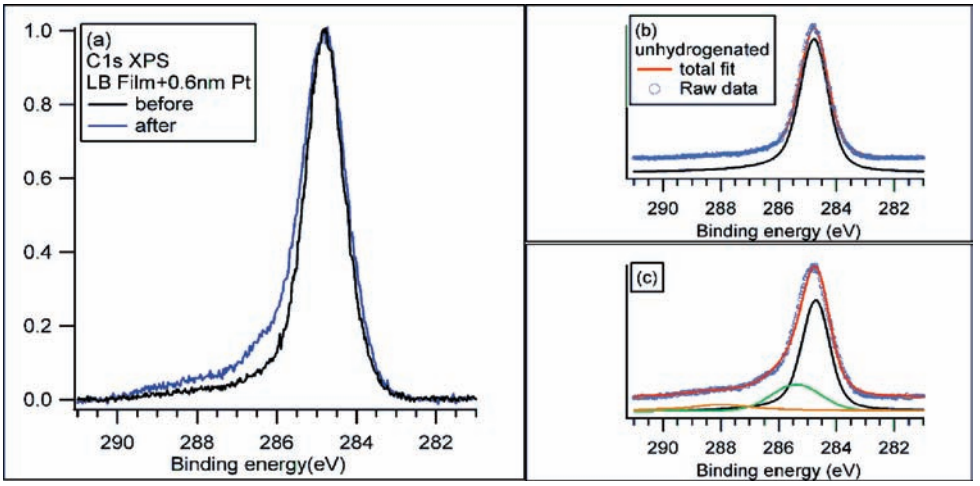

Figure 5. (a) C 1s XPS spectra before and after hydrogen exposure for an LB film with 6 Å Pt; the peak maxima of both spectra are normalized to enhance differences in the peak shapes. Gaussian−Lorentzian deconvolution (see text for details) of C 1s XPS spectra of the LB film (b) before and (c) after hydrogen charging: raw data (blue ○); total fit (red line); sp^2-C peak (black line); sp^3-C peak (green line); additional peak due to hydrogen-induced metal-to-semiconductor transition (orange line). Note that all peaks in (b) and (c) are offset downward from the raw data and the total fit. The incident photon energy is 400 eV.

before and after Pt deposition remain almost the same, implying that the sputtered Pt even for the LB films are not continuous but are in the form of catalyst particles dispersed on the nanotube surface. Hydrogen uptake by the Pt-SWNT composites has a strong dependence on the thicknesses of the SWNT mats (Figure 3b). The sparse SWNT LB films show an increase of more than an order of magnitude in normalized change in resistance values as compared to the HiPCO SWNT films spun-cast on glass. This dependence is attributed to the numerical density of Pt particles per area of the SWNT film exposed to hydrogenation, which is the least for the thick HiPCO films and highest for the LB films. Thus, for maximum hydrogen storage, it is necessary to obtain a uniform dispersion of monolayer thick unbundled SWNTs, doped with optimal size and density of Pt catalyst particles. This will ensure a high specific hydrogen uptake per weight of Pt-SWNT composite.

To understand the origin of resistance change upon hydrogen treatment, XPS measurements were performed before and after hydrogen exposure for CVD-grown (CVD) and LB-film samples with a nominal 6 Å thickness of deposited Pt. The C 1s spectra are shown in Figures 4 and 5, with the binding energy referenced to the Fermi level. The full-width at half-maximum (fwhm) of the C 1s spectra of the Pt-SWNT composites before hydrogen charging is 1.4 and 1.15 eV for the CVD-grown SWNTs (Figure 4a) and LB films (Figure 5a), respectively. The increased fwhm associated with CVD-grown samples as compared to the LB films could arise from a higher defect density or a different diameter distribution of the nanotubes we examined.

Peak fitting of all XPS C 1s spectra was performed after subtraction of a Shirley-type background.[25] For both the

dx.doi.org/10.1021/ja200403m |J. Am. Chem. Soc. 2011, 133, 5580–5586

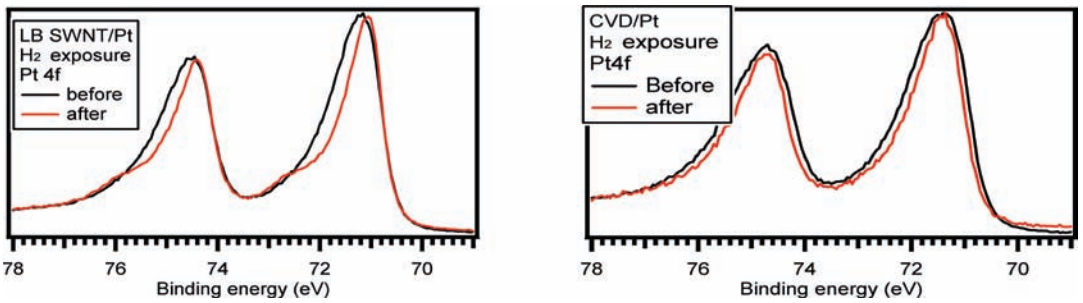

Figure 6. Pt 4f XPS spectra of an LB film Pt composite and CVD CNT-Pt composite before and after H_2 exposure; the photon energy is 400 eV.

CVD-grown and the LB-film composites, we were able to fit the spectra acquired before hydrogen exposure with a single asymmetric Gaussian−Lorentzian (GL) component centered at 284.8 eV (Figures 4b and 5b), which is consistent with an sp^2-hybridization of the C atoms;[7] the asymmetric tail of these spectra could be attributed to electron−hole pair excitations at the Fermi level arising from the metallic nature of the CNTs. The ratio of the peak to the tail intensity was maintained for all of the cases during the process of peak fitting.

After exposure to hydrogen at a pressure of 8.27 bar (120 psi) for 6 h, the fwhm of the C 1s spectrum of the CVD-grown SWNTs increased to 1.5 eV (Figure 4a), while that of the LB films increased to 1.35 eV (Figure 5a). Moreover, significant changes in the peak shape of the C 1s spectra are clearly visible in the high-binding-energy region: in addition to the previously observed peak associated with sp^2-hybridized carbon, a new feature, which we fitted using a symmetric GL with 2 eV fwhm, appears at ∼0.85 eV higher energy. This new spectral contribution is assigned to C atoms that have undergone rehybridization from sp^2 to sp^3 due to the breaking of C−C π-bonds and C−H bond formation[7,8] and can be seen as direct evidence for the proposed spillover effect. While the fwhm of the sp^3 peak of pure SWNTs following hydrogenation was reported to be 1 eV by Nikitin et al.,[7] we speculate that in the present study this feature is broadened by the strong interaction of the Pt nanoparticles with the nanotubes.

Furthermore, an additional peak at 288 eV (separated by ∼+3.3 eV from the main sp^2 C1s peak) can be detected for both hydrogenated samples, but with a higher intensity in the CVD-grown sample. A very similar feature can be observed when we hydrogenate pure SWNTs with atomic hydrogen;[9] in this case, the third feature is shifted from the sp^2-C peak by ∼ +2.1 eV. We conjecture that this additional peak arises from a metal-to-semiconductor transition of the nanotubes that is induced by hydrogenation. The decrease in conductivity accompanying such a transition can cause a reduction of the core-hole screening that increases the final-state energy by ∼2−3 eV. Alternatively, the creation of a band gap can give rise to a shakeup line: this results in an additional shift of the C 1s peak toward higher binding energies for a less screened final state. One might speculate that the additional peak at 288 eV could originate from a C−O species, introduced either by a reaction of SWNTs with oxygen, or by the adsorption of carbon monoxide, which is present in the residual gas of the UHV chamber, on the Pt nanoparticles. The former interpretation would be highly unreasonable given the strongly reducing conditions of hydrogen exposure. The latter, CO adsorption on Pt nanoparticles can be clearly ruled out by examining the Pt 4f region in the XPS. Chemisorbed CO on Pt bridge and on-top sites would cause chemical shifts of +0.7 and +1.5 eV with respect to the bulk peak of clean Pt, respectively.[26] Such features do not appear in our measurement after the hydrogenation of Pt-SWNT; instead, we observe further sharpening of the Pt 4f peaks upon hydrogen exposure (Figure 6). The sharpening could be explained by the process of removing adsorbed CO from the surface of Pt, replacing it with an adsorbed layer of hydrogen. We can thus confirm that the new feature at 288 eV originates from the SWNT metal-to-semiconductor transition caused by C−H bond formation. This finding is also in very good agreement with the conductivity decrease measured in situ.

By deconvoluting the XPS spectra, we can estimate the percentage of carbon atoms that have undergone a change from sp^2 to sp^3 hybridization, which can in turn be used to determine the hydrogen-weight capacity of the Pt-SWNT composites. The relative weights of the sp^2 (sp^3) peaks are 0.84 (0.17) for the LB-film composite and 0.87 (0.13) for the CVD-grown composite. The third peak at 288 eV has a relative weight of ∼0.05 in both samples. Because the fraction of hydrogenated carbon atoms is proportional to the relative peak intensity, we obtain atomic-hydrogen percentages of 16 ± 1.5 at. % for the LB film and 12 ± 1 at. % for the CVD-grown film (errors are given as standard deviation of the peak fits normalized to the total peak area). Because the hydrogen-weight capacity of a fully hydrogenated SWNT is 7.7 wt %, the weight-percentage hydrogen uptake is 1.2 wt % for LB films and 1 wt % for the CVD-grown films (excluding the weight of the deposited Pt nanoparticle catalyst).

These results indicate that it is possible to hydrogenate CNTs using molecular hydrogen and a Pt catalyst with the spillover mechanism. The bonding between Pt−C could involve the interaction of the π-electron system of the CNTs with the Pt-d states similar to what have been observed upon chemisorption of benzene on metal surfaces.[27−29] The observation that the Pt does not wet the nanotube, but rather aggregates into nanoparticles, is strong evidence the Pt−C bonds are not strong. The diffusion of hydrogen from the surface of the Pt nanoparticles to the CNTs may be facilitated by interaction between Pt and CNTs; theoretical studies can provide further insight in this regard.

Because the barrier for the diffusion of atomic hydrogen on SWNTs is quite large (∼0.7 eV),[9] it is likely that in the composites studied here only a small region close to the Pt nanoparticles is hydrogenated. While longer diffusion lengths can be achieved by using higher temperatures, we expect that such conditions will significantly improve hydrogen storage only if hydrogen desorption from the Pt nanoparticles is counteracted by increasing the pressure. To achieve 100% hydrogenation via hydrogen spillover, it is also essential that the Pt catalyst is very

evenly dispersed over the surface of the SWNTs; this is only possible with nonbundled nanotubes, for which a high Pt-to-C dispersion can be achieved.

4. CONCLUSIONS

In the present Article, we have demonstrated, using both in situ conductivity and ex situ XPS studies of Pt-SWNTs, that the spillover mechanism is responsible for hydrogenation of Pt-SWNT composites using molecular hydrogen. We have also shown that these materials store hydrogen by chemisorption, that is, the formation of stable C−H bonds. CNTs doped with suitable metal catalysts consequently represent viable materials for hydrogen storage. We have further identified that there is an optimal platinum catalyst particle size of ∼2 nm (which corresponds to nominal thickness of 6 Å) that needs to be deposited onto the SWNTs for maximal hydrogen uptake, which corresponds well with the previously reported value.[24] The hydrogen uptake due to exposure to molecular hydrogen of ∼8.27 bar, quantified by XPS, indicates 1.2 wt % hydrogen storage for LB-film composites and 1 wt % for CVD-grown CVD composites. This storage capacity may be increased by improving the kinetics of atomic-hydrogen diffusion from the Pt catalyst to the SWNT support and also by employing nonbundled CNTs with an increased Pt-to-C dispersion.

■ ASSOCIATED CONTENT

Supporting Information. Details on in situ electrical conductivity measurement setup and TEM images of SWNTs with different nominal thickness of deposited Pt. This material is available free of charge via the Internet at http://pubs.acs.org.

■ AUTHOR INFORMATION

Corresponding Author
nilsson@slac.stanford.edu

■ ACKNOWLEDGMENT

This work was supported by the Global Climate and Energy Project operated by Stanford University and carried out at the Stanford Synchrotron Radiation Lightsource, a National User Facility operated by Stanford University on behalf of the U.S. Department of Energy, Office of Basic Energy Sciences.

■ REFERENCES

(1) Dillon, A. C.; Jones, K. M.; Bekkedahl, T. A.; Kiang, C. H.; Bethune, D. S.; Heben, M. J. *Nature (London)* **1997**, *386*, 377–379.
(2) Park, S.; Srivastava, D.; Cho, K. *Nano Lett.* **2003**, *3*, 1273–1277.
(3) Nikitin, A.; Zhang, Z.; Nilsson, A. *Nano Lett.* **2009**, *9*, 1301–1306.
(4) Zhang, G.; Qi, P.; Wang, X.; Lu, Y.; Mann, D.; Li, X.; Dai, H. *J. Am. Chem. Soc.* **2006**, *128*, 6026–6027.
(5) Ruffieux, P.; Groning, O.; Bielmann, M.; Mauron, P.; Schlapbach, L.; Groning, P. *Phys. Rev. B* **2002**, *66*, 245416.
(6) Khare, B. N.; Meyyappan, M.; Cassell, A. M.; Nguyen, C. V.; Han, J. *Nano Lett.* **2002**, *2*, 73.
(7) Nikitin, A.; Ogasawara, H.; Mann, D.; Denecke, R.; Zhang, Z.; Dai, H.; Nilsson, A. *Phys. Rev. Lett.* **2005**, *95*, 225507.
(8) Tokura, A.; Maeda, F.; Teraoka, Y.; Yoshigoe, A.; Takagi, D.; Homma, Y.; Watanabe, Y.; Kobayashi, Y. *Carbon* **2008**, *46*, 1903–1908.
(9) Nikitin, A.; Li, X.; Zhang, Z.; Ogasawara, H.; Dai, H.; Nilsson, A. *Nano Lett.* **2008**, *8* (1), 162–167.
(10) Nikitin, A.; Näslund, L. Å.; Zhang, Z.; Nilsson, A. *Surf. Sci.* **2008**, *602*, 2575–2580.
(11) Somorjai, G. A. *Introduction to Surface Chemistry and Catalysis*; Wiley-Interscience: New York, 1994.
(12) Lee, Y.-W. Ph.D. Thesis, Stanford University, 2009.
(13) Lee, Y.-W.; Clemens, B. M.; Gross, K. J. *J. Alloys Compd.* **2008**, *452*, 410–413.
(14) Zacharia, R.; Kim, K. Y.; Fazle Kibria, A. K. M.; Nahm, K. S. *Chem. Phys. Lett.* **2005**, *412*, 369–375.
(15) Zacharia, R.; Rather, S.; Hwang, S. W.; Nahm, K. S. *Chem. Phys. Lett.* **2007**, *434*, 286–291.
(16) Wang, L.; Yang, R. T. *J. Phys. Chem. C* **2008**, *112*, 12486–12494.
(17) Mitchell, P. C. H.; Ramirez-Cuesta, A. J.; Parker, S. F.; Tomkinson, J.; Thompsett, D. *J. Phys. Chem. B* **2003**, *107*, 6838–6845.
(18) Contescu, C. I.; Brown, C. M.; Liu, Y.; Bhat, V. V.; Gallego, N. C. *J. Phys. Chem. C* **2009**, *113*, 5886–5890.
(19) Lin, C.; Yang, Z.; Xu, T.; Zhao, Y. *Appl. Phys. Lett.* **2008**, *93*, 233110.
(20) Lachawiec, A. J., Jr.; Yang, R. T. *Langmuir* **2008**, *24*, 6159–6165.
(21) Li, X.; Zhang, L.; Wang, X.; Shimoyama, I.; Sun, X.; Seo, W.-S.; Dai, H. *J. Am. Chem. Soc.* **2007**, *129*, 4890–4891.
(22) Kataura, H.; Kumazawa, Y.; Maniwa, Y.; Umezu, I.; Suzuki, S.; Ohtsuka, Y.; Achiba, Y. *Synth. Met.* **1999**, *103*, 2555–2558.
(23) Gorodetskii, V. V.; Matveev, A. V.; Cobden, P. D.; Nieuwenhuys, B. E. *J. Mol. Catal. A: Chem.* **2000**, *158*, 155–158.
(24) Bhowmick, R. Ph.D. Thesis, Stanford University, 2010; Chapter 7.
(25) Shirley, D. A. *Phys. Rev. B* **1972**, *5*, 4709–4714.
(26) Björneholm, O.; Nilsson, A.; Tillborg, H.; Bennich, P.; Sandell, A.; Hernnäs, B.; Puglia, C.; Mårtensson, N. *Surf. Sci.* **1994**, *315*, L983–L989.
(27) Weinelt, M.; Wassdahl, N.; Wiell, T.; Karis, O.; Hasselström, J.; Bennich, P.; Nilsson, A.; Stöhr, J.; Samant, M. *Phys. Rev. B* **1998**, *58*, 7351–7360.
(28) Triguero, L.; Föhlisch, A.; Väterlein, P.; Hasselström, J.; Weinelt, M.; Pettersson, L. G. M.; Yi Luo, H.; Ågren; Nilsson, A. *J. Am. Chem. Soc.* **2000**, *122*, 12310–12316.
(29) Nilsson, A.; Pettersson, L. G. M. *Surf. Sci. Rep.* **2004**, *55*, 49–167.